JOURNAL OF SOLID STATE CHEMISTRY **97**, 199–211 (1992)

A Single Crystal X-ray and High Resolution Electron Microscope Study of $Pb_5Sb_6S_{14}$

A. SKOWRON AND I. D. BROWN

Institute for Materials Research, McMaster University, 1280 Main St. West, Hamilton, Ontario, Canada L8S 4M1

AND R. J. D. TILLEY,

Division of Materials, School of Engineering, University of Wales, P.O. Box 914, Cardiff CF2 1XH, United Kingdom

Received January 23, 1991; in revised form September 24, 1991

The structure of $Pb_5Sb_6S_{14}$, first observed by HREM, has been refined by single crystal X-ray diffraction. It is a higher homologue of robinsonite, $Pb_4Sb_6S_{13}$, with $a = 28.367(8)$ Å, $b = 4.024(1)$ Å, $c = 22.044(7)$ Å, $\alpha = 89.59(2)$, $\beta = 92.28(3)$, $\gamma = 89.93(2)$, space group $I\bar{1}$, $Z = 4$. $Pb_5Sb_6S_{14}$ is built from two different ribbons composed of square pyramidal (Pb, Sb)S_5 groups with the narrow ribbon identical to that in robinsonite and the other ribbon one pyramid wider. HREM studies indicate that during electron microscope observation $Pb_5Sb_6S_{14}$ decomposes into three different polymorphs of PbS. High resolution electron micrographs allow models to be proposed for the transformations.

Introduction

$Pb_5Sb_6S_{14}$ was first reported by Wang (*1*). He chose a triclinic unit cell for the structure with $a = 18.40$ Å, $b = 17.69$ Å, $c = 4.01$ Å, $\alpha = 96°17'$, $\beta = 96°04'$, $\gamma = 103°39'$ to compare it with the unit cell of robinsonite, $Pb_4Sb_6S_{13}$, and reported a striking resemblance in the single crystal diffraction patterns of these two phases. He also stated that the true symmetry of $Pb_5Sb_6S_{14}$ might be monoclinic, like robinsonite, and gave the lattice parameters for the monoclinic setting as $a = 21.98$ Å, $b = 35.12$ Å, $c = 4.02$ Å, $\gamma = 126°15'$ for an *A*-centered lattice. The reported stability range was 786–865 K, and between 786–856 K the phase coexisted with robinsonite.

The present investigation was initiated when $Pb_5Sb_6S_{14}$ was found in an electron microscope study of phases in the PbS–Sb_2S_3 system. High resolution electron micrographs allowed us to derive a model for the structure and indicated that the phase decomposed under electron irradiation to a galena-like structure. Electron microscopy did not, however, allow us to obtain precise crystallographic details, and hence we undertook an investigation using X-ray diffraction. The present paper describes both studies.

Experimental

Preparation

$Pb_5Sb_6S_{14}$ was synthetized from elemental lead, antimony, and sulfur of "Specpure" grade, supplied by Johnson Matthey, Ltd.

0022-4596/92 $3.00

The sample was prepared by weighing the elements in proportions corresponding to 60 mole% of PbS, melting the mixture in an evacuated silica tube at 1150 K for 1 day, and subsequently annealing at 723 K for 2 weeks. The samples yielded a mass of very small acicular crystals which were characterized by powder X-ray diffraction and electron microscopy.

To grow single crystals the melt was quenched and the resulting ingot ground, pressed into a 1-g pellet and, after addition of approximately 1 mg of I_2, annealed in a two-zone horizontal furnace for 3 days. The pellet was placed at the end of the 20-cm ampoule, where the temperature was held at 860 K to avoid the formation of robinsonite. The other end was kept at 875 K. Acicular crystals grew in various parts of the ampoule, most often near the cooler end. A needle shaped crystal, 0.1 mm × 0.6 mm × 0.15 mm, was mounted with the needle axis along the goniometer axis for the X-ray study on the Syntex $P2_1$ diffractometer.

Single Crystal X-ray Diffraction

The unit cell parameters were obtained from the single crystal by a least square refinement using the Bragg angles of 15 well-centered reflections in the range indicated in Table I, which also gives other experimental parameters of the structure determination. The systematic absences, hkl: $h + k + l = 2n + 1$, and the diffraction symmetry found on precession photographs, indicate the space group $I\bar{1}$, but the intensities showed a pseudo-mirror plane normal to b. We chose to use the body-centered space group rather than the more usual primitive setting, as this reflected the pseudo-monoclinic cell.

The initial atomic positions, found by direct methods using SHELXS, were refined using SHELX76 by full matrix least squares with anisotropic atomic displacement parameters for all the atoms and with mixed occupancies for the metal sites. Complex scattering factors for neutral atoms were taken from International Tables for X-ray Crystallography (*2*). The intensities were weighted by $w = k/[\sigma^2(F_o) + gF_o^2]$, where k refined to 1.07, g was fixed at 0.0006, and $\sigma(F_o)$ was the uncertainty derived from the counting statistics. The Pb occupation numbers of sites 14 and 15 and Sb occupation numbers of sites 3, 4, and 10 quickly refined to values close to 1.0 and were kept fixed at this value in the subsequent stages of the refinement. Because of large positive peaks in the electron density difference maps and large thermal displacement parameters in the b-direction of four sites (10, 11, 12, 13) we split these positions in b-direction and, by trial and error, put Pb in sites denoted 11a, 12a, and 13a, and Sb in sites 10a, 10b, 11b, 12b, and 13b, keeping the total occupation of a site equal 1.0. The y-coordinates of the split positions were heavily correlated in the refinement, and they were also correlated with the thermal displacement parameters in this direction (correlation factors between 0.60–0.91). The refinement converged to $wR = 0.087$, $R = 0.099$, and $s = 1.74$. The program did not permit a constraint to be put on the total number of Pb or Sb atoms in the unit cell, and the refined occupation numbers, shown in column 2 of Table II, result in a formula of $Pb_{4.68}Sb_{6.32}S_{14}$, which is appreciably different from the electrically neutral formula $Pb_5Sb_6S_{14}$. In order to clarify this discrepancy we determined an independent set of occupation numbers using the bond–valence method as described by Skowron and Brown (*3*). In this method the refined atomic parameters were used to calculate bond lengths (r) from which bond–valences (s) were calculated using the equation

$$s = \exp((r_o - r)/0.37), \qquad (1)$$

where $r_o = 2.541$ Å for Pb–S and $r_o = 2.530$ Å for Sb–S bonds. The valence analysis is presented in Table III, and both the X-ray and valence occupation numbers for Sb are compared in Table II. The Pb occupation

TABLE I

STRUCTURE PARAMETER FOR $Pb_5Sb_6S_{14}$

Syntex $P2_1$ diffractometr		
λ (Mo$K\alpha$)	0.71069 Å	
Space group		$I\bar{1}$
Lattice parameters (Å)		
this study	a = 28.367(8)	α = 89.59(2)
	b = 4.024(1)	β = 92.28(3)
	c = 22.044(7)	γ = 89.93(2)
Wang (*1*), after converting to the I setting	a = 28.44 Å	α = 90°
	b = 4.02 Å	β = 92°
	c = 21.98 Å	γ = 90°
Volume ($Å^3$)		2514
Calculated density (g/cm^3)		5.86
Z		4
Reflections used to determine lattice parameters		$19° < 2\theta < 24°$
Standard reflections		13 0 3, −13 1 −2
e.s.d. of standard reflections (%)		3.0, 3.0
No. of standard reflection measurements		95, 95
Range of measured reflections		$-33 \leq h \leq 32$
		$-4 \leq k \leq 4$
		$0 \leq l \leq 26$
No. of reflections measured		4444
No of reflections used in the refinement		4444
Linear absorption coefficient μ (mm^{-1})		39.1
No. of reflections used in psi-scan		21
Absorption correction: maximum; reflection		4.10; 1 2 1
Final R; R_w; s		0.088; 0.100; 1.74
Shift/error in final cycle: maximum		0.011
average		0.002
Number of variables refined		245
Residual electron density: maximum ($eÅ^{-3}$)		4.3
minimum		−3.4

numbers are given by the difference between the Sb figure quoted and 100%.

Because the occupation numbers determined from the bond valences correspond to an electrically neutral crystal we consider these values to be more reliable. We used the valence derived values given in column 3 of Table II as fixed parameters in SHELX76 and refined all positional and atomic displacement parameters to obtain the residuals listed in Table I. This refinement was used to generate the final atomic coordinates listed in Table IV. The anisotropic atomic displacement parameters are given in Table V, and the interatomic distances in Table VI. Copies of the list of observed and calculated structure factors can be obtained from either of the first two authors.

Electron Microscope Study

Electron diffraction and high resolution imaging studies were performed using a JEOL 200CX electron microscope fitted with a high resolution objective lens pole piece (C_s = 1.2 mm) and a top-entry, double-tilt goniometer stage, (±10°), operated at an accelerating voltage of 200 kV. Specimens suitable for electron microscopy were prepared by crushing crystals in an agate mortar under *n*-butanol and allowing

TABLE II

PERCENTAGE OF Sb ON CATION SITES IN $Pb_5Sb_6S_{14}$

Site	X-ray	Bond valence
M(1)	66	55 (70)[a]
M(2)	21	10
M(3)	100	100
M(4)	100	100
M(10)[b]	100	100
M(11)b[c]	82	80
M(12)b	75	70
M(13)b	65	65 (50)[b]
M(14)	0	0
M(15)	0	0
M(16)	23	20
Formula	$Pb_{4.68}Sb_{3.32}S_{14}$	$Pb_5Sb_6S_{14}$

[a] The occupation numbers in cation sites 1 and 13 were changed slightly from the values calculated using the bond valence method (shown in brackets in column 3) to obtain a lower residual and lower thermal displacement parameters for the site 13 in the *b*-direction.

[b] This site is split into 10a and 10b both occupied by 50% Sb.

[c] Lead occupies sites M(11)a, M(12)a, and M(13)a.

a drop of the resultant suspension to dry on a copper grid coated with a holey carbon film. Image astigmatism and beam alignment were corrected by direct observation of support film granularity at typical magnifications of ×600,000 to ×750,000. Exposure times were typically 4 sec at a magnification of ×750,000. Images were recorded at a series of defocus steps near the Scherzer defocus ($\Delta f = -1.2C^{1/2}\lambda^{1/2} = -660$ Å) to obtain optimum phase contrast. Under these conditions the image of a sufficiently thin crystal corresponds to the projected charge density at a resolution limit of approximately $0.67C_s^{1/4}\lambda^{3/4}$ ($\simeq$2.5 Å) (*4*). Electron diffraction patterns and images were calculated using the EMS package of programs (*13*).

Description of the Structure

The structure of $Pb_5Sb_6S_{14}$ (Figs. 1 and 2a) is closely related to robinsonite, $Pb_5Sb_6S_{13}$ (*3*), Fig. 2b, and consists of ribbons built of back-to-back square pyramidal (Pb, Sb)S_5 groups. The ribbons extend indefinitely in the *b*-direction. They are one pyramid thick and have two different widths. The narrow ribbon, in which the width equals twice the basal distance of the (Pb, Sb)S_5 pyramid, is identical with the Sb_4S_6 building unit in stibnite, Sb_2S_3 (*5*), and robinsonite. The wide ribbon, where the width equals seven times the basal distance of the pyramid, can be formed by incorporation of five pairs of back-to-back PbS_5 pyramids into the middle of the narrow ribbon. Alternatively, the structure of $Pb_5Sb_6S_{14}$ can be obtained directly from the structure of robinsonite by inserting an additional pair of back-to-back PbS_5 pyramids into the middle of the wide ribbon of robinsonite (compare Figs. 2a and 2b).

The stoichiometry of $Pb_5Sb_6S_{14}$ can be determined by the total number of PbS units that have to be incorporated into the wide ribbon as

$$2\underbrace{[Sb_2S_3 + Sb_2S_3]}_{\text{narrow ribbon}} + \underbrace{[Sb_2S_3 + (PbS)_{10} + Sb_2S_3]}_{\text{wide ribbon}} = 2\ Pb_5Sb_6S_{14}.$$

In the crystal, however, the Pb atoms are not found only in the middle of the wide ribbons. Sb prefers the five coordinated sites which occur at the places where each ribbon faces a parallel ribbon, while Pb favors the higher coordinated sites where the face of one ribbon meets the edge of a neighbor.

The mirror plane normal to the short *b*-axis, present in robinsonite, is absent in $Pb_5Sb_6S_{14}$, as indicated by the absence of mirror symmetry in precession photographs. The departure from the monoclinic symmetry is only slight, and the *y*-coordinates all refined to values close to the pseudo-mirror planes at 0 or $\frac{1}{2}$. Moreover, the cations (M 10, 11, 12, 13) in the wide

TABLE III

VALENCE ANALYSIS OF $Pb_5Sb_6S_{14}$

	M(1)	M(2)	M(3)	M(4)	M(10)	M(11)	M(12)	M(13)	M(14)	M(15)	M(16)	Σs
%Sb	66	21	100	100	100	82	75	65	0	0	23	
S(1)	0.21 + 0.49			1.20						0.17		−2.07
S(2)		0.5	0.63	0.62								−1.75
S(3)		0.43 + 0.11	1.28						0.45			−2.27
S(4)	0.11 + 0.26	0.63 + 0.16		1.26								−2.42
S(5)	0.58 + 1.10										0.58 + 0.08	−2.34
S(6)			1.32						0.41	0.16		−1.89
S(10)					1.27						0.69 + 0.20	−2.16
S(11)						0.02 + 0.89				0.69	0.39 + 0.11	−2.10
S(12)							0.19 + 0.69		0.66	0.60		−2.14
S(13)								0.64 + 1.21	0.25			−2.10
S(14)							0.29 + 0.91	0.27 + 0.34	0.15			−1.96
S(15)						0.15 + 0.67	0.14 + 0.42			0.39		−1.77
S(16)					0.31 + 0.15	0.17 + 0.70					0.34 + 0.01	−1.68
S(17)		0.21 + 0.06			1.15 + 0.47			0.06 + 0.09				−2.04
Σs	2.75	2.10	3.23	3.08	3.35	2.60	2.64	2.61	1.92	2.01	2.40	
V	2.66	2.21	3.00	3.00	3.00	2.82	2.75	2.65	2.00	2.00	2.23	

Note. The bond valences are an average of the valences calculated as Pb–S and Sb–S weighted according to the X-ray occupation numbers. V is the atomic valence similarly weighted.

TABLE IV

Atomic Coordinates for $Pb_5Sb_6S_{14}$

	x	y	z
M(1)	0.7005(1)	0.0005(4)	0.6880(1)
M(2)	0.6628(1)	0.0069(3)	0.4937(1)
M(3)	0.5396(1)	0.5129(6)	0.4293(1)
M(4)	0.5829(1)	0.5076(6)	0.6199(1)
M(10)a	0.8038(1)	0.9726(26)	0.4761(1)
M(10)b	0.8038(1)	0.0823(18)	0.4761(1)
M(11)a	0.9500(1)	0.9521(32)	0.5485(1)
M(11)b	0.9500(1)	0.0602(8)	0.5485(1)
M(12)a	0.9067(1)	0.0277(35)	0.3792(1)
M(12)b	0.9067(1)	0.9347(25)	0.3792(1)
M(13)a	0.7667(1)	0.0258(55)	0.3265(1)
M(13)b	0.7667(1)	0.9440(45)	0.3265(1)
M(14)	0.8864(1)	0.4943(3)	0.2026(1)
M(15)	0.9813(1)	0.5088(3)	0.7122(1)
M(16)	0.8397(1)	0.5110(3)	0.6346(1)
S(1)	0.6052(2)	0.9995(19)	0.6989(4)
S(2)	0.5678(2)	0.0023(19)	0.5223(4)
S(3)	0.6225(2)	0.5074(16)	0.4038(3)
S(4)	0.6643(2)	0.5020(18)	0.5873(3)
S(5)	0.6981(2)	0.4988(21)	0.7670(3)
S(6)	0.5230(2)	0.0083(19)	0.3507(3)
S(10)	0.7811(2)	0.0188(19)	0.5813(4)
S(11)	0.9199(2)	0.0104(18)	0.6532(3)
S(12)	0.9411(2)	0.9908(17)	0.2738(4)
S(13)	0.7942(3)	0.9977(21)	0.2128(4)
S(14)	0.8475(3)	0.4950(20)	0.3384(4)
S(15)	0.9836(3)	0.4902(19)	0.4093(4)
S(16)	0.8812(3)	0.5149(19)	0.5195(4)
S(17)	0.7462(3)	0.5151(24)	0.4495(4)

ribbons were found to be split in the *b*-direction over two sites, and the antimony atoms in the narrow ribbons (M 3, 4,) have high U_{22} atomic displacement parameters (0.057 Å^2) suggestive of a small splitting. The atoms on sites 3 and 4 were left unsplit because the atomic displacement parameters in these atoms are approximately 0.03–0.05 Å^2 smaller than those in sites 10–13 before introducing the splitting. Finding six of the eleven cations split in a crystal with the triclinic symmetry suggests that microtwinning might be present, but because of the high correlation between parameters during the refinement it is not possible to construct a reliable model. This kind of twinning will not be visible in electron micrographs viewed along the *b*-axis, but could be imaged in other projections, suggesting that further study might be appropriate.

Three related types of structures are commonly used as parent or archetypal structures in interpretation of the structures of ribbon-like lead–antimony sulphides (*6, 7*). These are: the galena structure (PbS with the NaCl structure), the thallium iodide structure (B33) (*9*), and the SnS (B16) structure (*10, 11, 12*). Both the TlI and SnS structures can be derived from the galena structure. TlI results when a 2-Å shear along [010] in the (100) plane is introduced into the lattice. This breaks the cation octahedra into square pyramids having five short bonds within the pyramids and two long bonds across the shear plane to the neighboring pyramids. When

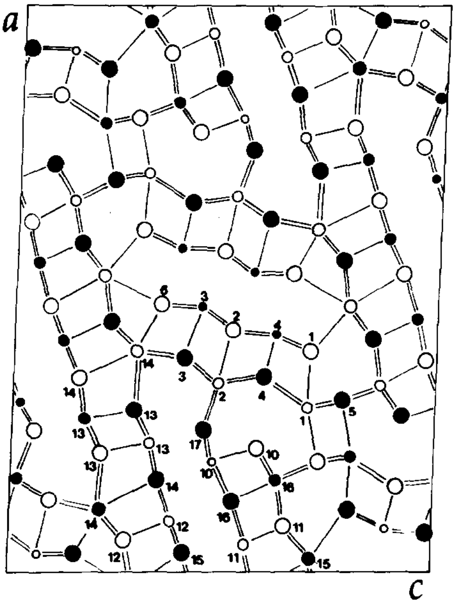

Fig. 1. The unit cell of $Pb_5Sb_6S_{14}$ projected down [010]. In order of decreasing size, the circles denote S, Pb, mixed sites, and Sb. Atoms at $y \cong 0.0$ and $y \cong 0.5$ are indicated by open and filled circles, respectively.

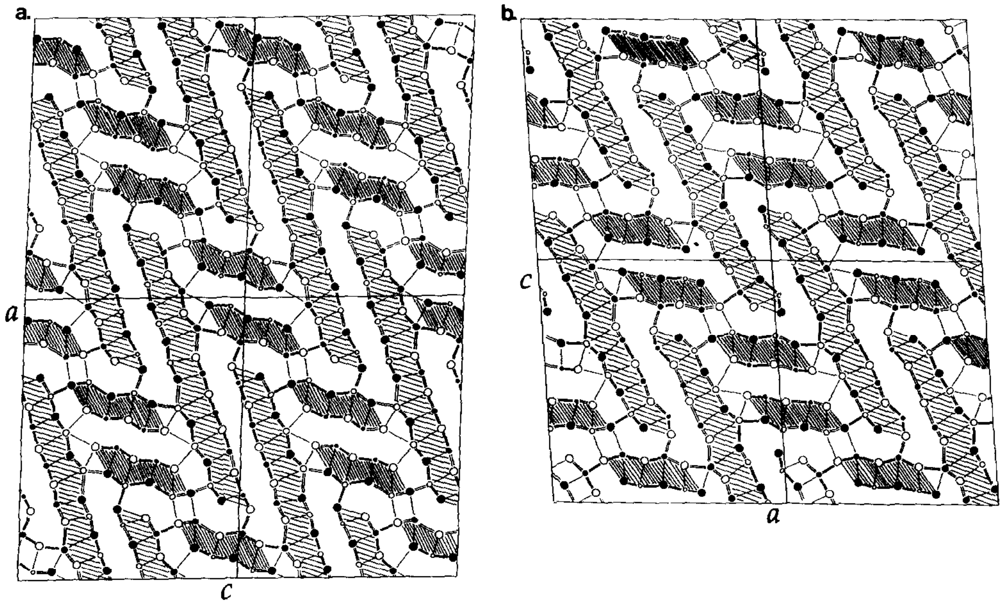

FIG. 2. Four unit cells of the crystal structure of (a) $Pb_5Sb_6S_{14}$ and (b) $Pb_4Sb_6S_{13}$ (robinsonite) projected down [010] with the wide and narrow ribbons indicated by coarse and fine ruling, respectively. Conventions for indicating the atoms are the same as in Fig. 1.

alternate unit cells are sheared the structure is broken into sheets similar to the ribbons of robinsonite. The SnS structure is then obtained from TlI by displacing the cation from the center of the base of the pyramid in such a way as to break the mirror symmetry perpendicular to (010) giving two short and two long basal bonds. This is accompanied by the square base of the pyramid becoming rectangular.

SnS undergoes a phase transition on heating to 878 K from the SnS to the TlI structure. Wiedemeier and von Schnering (*11*) investigated the transition $SnS_{SnS\ type} \rightarrow SnS_{TlI\ type}$ and found that the transformation occurs in two steps, the first of which begins approximately 200° below T_c and involves a continuous displacement of the cations toward the centers of the pyramids together with a continuous change in the shape of the pyramid bases from rectangular (3.98 × 4.33 Å) to square. The second step starts about 5° below T_c and involves a distortion of the square base to a rectangle (4.18 × 4.15 Å) elongated in the opposite sense.

There has been some question as to whether robinsonite has a mirror plane normal to the *b*-axis, resulting in the ribbons having the TlI structure. Wang (*1*) suggested that the mirror plane is not part of the true symmetry of the crystal and might be caused by an intimate twinning of domains in which the cations are displaced from the base centers in opposite directions. This view is endorsed by Makovicky (*8*), who also assumes that the SnS structure is the archetype for the robinsonite ribbons.

If twinning were indeed present in robinsonite it should be recognizable by atom splitting or elongation in the X-ray refinement as it is in $Pb_5Sb_6S_{14}$. But the temperature factors show no anomalies. The striking differences between the refinements of the two structures suggest that robinsonite has true monoclinic symmetry based on the TlI

TABLE V

ANISOTROPIC THERMAL DISPLACEMENT PARAMETERS FOR $Pb_5Sb_6S_{14}$ (Å^2)

	U_{11}	U_{22}	U_{33}	U_{12}	U_{13}	U_{23}
M(1)	0.045(1)	0.029(1)	0.040(1)	0.0001(7)	−0.0076(8)	0.0009(7)
M(2)	0.043(1)	0.032(1)	0.031(1)	0.0011(5)	0.0032(6)	0.0001(6)
M(3)	0.022(1)	0.057(1)	0.045(1)	−0.0069(3)	0.0098(9)	0.0022(11)
M(4)	0.023(1)	0.056(1)	0.047(2)	−0.0005(1)	0.0099(10)	0.0016(12)
M(10)[a]	0.036(1)	0.035(6)	0.028(1)	0.0061(8)	0.0091(10)	0.0028(9)
M(11)	0.039(1)	0.037(3)	0.040(1)	0.0061(8)	0.0101(10)	0.0028(9)
M(12)	0.032(1)	0.030(5)	0.044(1)	−0.0066(9)	0.0076(9)	−0.0035(12)
M(13)	0.029(1)	0.057(9)	0.055(1)	−0.0059(9)	−0.0017(9)	−0.0064(2)
M(14)	0.030(1)	0.030(1)	0.039(1)	−0.0006(5)	−0.0059(5)	0.0014(6)
M(15)	0.028(1)	0.029(1)	0.031(7)	0.0000(5)	0.0016(5)	−0.0001(5)
M(16)	0.027(1)	0.031(1)	0.044(1)	−0.0004(5)	0.0099(6)	−0.0007(6)
S(1)	0.017(3)	0.041(4)	0.025(4)	0.0017(28)	0.0082(29)	0.0005(34)
S(2)	0.016(3)	0.036(4)	0.034(5)	−0.0051(27)	0.0075(30)	0.0025(36)
S(3)	0.017(3)	0.018(3)	0.026(4)	−0.0002(24)	0.0041(27)	0.0013(29)
S(4)	0.013(3)	0.033(4)	0.021(4)	−0.0004(25)	0.0005(25)	−0.0019(30)
S(5)	0.027(4)	0.051(5)	0.018(4)	−0.0005(33)	0.0038(30)	0.0025(35)
S(6)	0.018(3)	0.042(4)	0.018(4)	−0.0009(28)	0.0009(27)	−0.0030(32)
S(10)	0.026(4)	0.035(4)	0.027(4)	0.0033(30)	0.0063(30)	0.0026(34)
S(11)	0.022(3)	0.031(4)	0.024(4)	0.0015(28)	0.0008(29)	0.0008(32)
S(12)	0.015(3)	0.026(3)	0.038(5)	−0.0014(26)	−0.0018(30)	−0.0011(33)
S(13)	0.028(4)	0.050(5)	0.023(4)	−0.0029(33)	0.0050(31)	0.0035(37)
S(14)	0.034(4)	0.037(4)	0.030(5)	−0.0021(32)	0.0117(34)	−0.0014(36)
S(15)	0.045(4)	0.024(4)	0.029(4)	−0.0030(31)	0.0087(35)	0.0074(33)
S(16)	0.040(4)	0.030(4)	0.030(4)	0.0044(32)	0.0119(34)	0.0033(34)
S(17)	0.028(4)	0.064(6)	0.037(5)	0.0024(37)	0.0103(36)	0.0124(45)

[a] Although the sites 10–13 are split, the thermal displacement parameters have been constrained to have the same value for both sites.

archetype but that the ribbons in $Pb_5Sb_6S_{14}$ have an SnS distortion with micro-twinning or some similar disorder.

Electron Microscopy

Figure 3a shows a high resolution electron micrograph of a thin crystal fragment of $Pb_5Sb_6S_{14}$. The structure is projected down the short *b*-axis, and the contrast can be interpreted directly as projected charge density. The metal–metal distances in the ribbons are approximately 4.0 Å (parallel to the face of ribbon) and 3.7 Å (diagonally across the ribbon). These distances are resolved in the HREM image, and the metal atoms appear as dark spots in the thinnest parts of the crystal. The wide ribbons are very clearly recognizable, while the narrow ribbons are less well resolved, compare Figs. 2a and 3a. The lattice images were calculated using the EMS package of programs (*13*), and the crystallographic data given in Tables II, IV, and V. The images, presented in Fig. 3b, show the effect of variation of crystal thickness, defocus, and objective aperture size. The best fit between the calculated images and those observed at the edges of the crystal is obtained for the conditions 5 unit cells thickness, 700 Å defocus, and 100 Å^{-1} objective aperture. The alternate gray and white strips visible in the thicker parts of the crystal are not mirrored exactly in the simulations, but the contrast

TABLE VI

BOND DISTANCES (Å) LESS THAN 3.6 Å IN $Pb_5Sb_6S_{14}$

Narrow ribbon		Wide ribbon	
M(1)–S(5)	2.660(8)	M(10)a–S(10)	2.437(9)
S(5)	2.669(8)	S(17)	2.516(12)
S(1)	2.725(7)	S(17)	2.776(12)
S(5)	3.006(7)	S(16)	2.994(10)
S(4)	3.134(7)	S(16)	3.214(11)
S(4)	3.143(7)		
S(10)	3.345(8)		
M(2)–S(2)	2.792(7)	M(10)b–S(10)	2.444(9)
S(4)	2.868(7)	S(17)	2.444(10)
S(4)	2.895(7)	S(17)	2.854(11)
S(3)	3.015(7)	S(16)	2.932(9)
S(3)	3.018(7)	S(16)	3.281(11)
S(17)	3.263(9)		
S(17)	3.304(9)		
M(3)–S(3)	2.441(6)	M(11)a–S(11)	2.504(8)
S(6)	2.670(8)	S(16)	2.686(11)
S(6)	2.699(8)	S(15)	2.729(11)
S(2)	2.929(8)	S(16)	3.040(12)
S(2)	2.988(8)	S(15)	3.051(12)
M(4)–S(4)	2.446(7)	M(11)b–S(11)	2.501(8)
S(1)	2.694(8)	S(16)	2.733(8)
S(1)	2.743(8)	S(15)	2.748(8)
S(2)	2.951(8)	S(16)	2.988(8)
S(2)	2.980(8)	S(15)	3.030(8)
		M(12)a–S(12)	2.560(8)
		S(14)	2.635(11)
		S(14)	2.867(12)
		S(15)	2.905(11)
		S(15)	3.143(11)
		M(12)b–S(12)	2.564(8)
		S(14)	2.577(9)
		S(15)	2.877(9)
		S(14)	2.931(9)
		S(15)	3.174(9)
		M(13)a–S(13)	2.658(9)
		S(13)	2.700(19)
		S(13)	2.835(19)
		S(14)	2.974(17)
		S(14)	3.136(18)
		S(17)	3.421(17)
		S(17)	3.469(17)
		M(13)b–S(13)	2.603(17)
		S(13)	2.664(9)
		S(14)	2.924(15)
		S(13)	2.940(18)
		S(14)	3.191(17)
		S(17)	3.268(17)
		S(17)	3.332(17)
		M(14)–S(6)	2.868(7)
		S(12)	2.945(7)
		S(12)	2.963(7)
		S(3)	3.087(7)
		S(3)	3.096(7)
		S(14)	3.234(8)
		S(13)	3.308(8)
		S(13)	3.324(8)
		M(15)–S(15)	2.894(9)
		S(11)	2.928(7)
		S(11)	2.937(7)
		S(12)	2.988(7)
		S(12)	2.990(7)
		S(1)	3.199(7)
		S(6)	3.231(7)
		M(16)–S(10)	2.814(8)
		S(16)	2.839(9)
		S(10)	2.858(8)
		S(11)	3.050(7)
		S(11)	3.053(7)
		S(5)	3.149(8)
		S(5)	3.200(8)

in the 20 cells 700 Å defocus image is close to that observed.

The samples were found to be very sensitive to the electron beam and during examination many crystal fragments decomposed. The process was usually rapid and occurred first at the edges of the crystal flakes. Figures 4 and 5 show the micrographs of two regions in a $Pb_5Sb_6S_{14}$ crystal which has partly decomposed into other structures.

The first of these structures, visible on both micrographs and labeled A, consists of ribbons, widened into sheets which follow the direction of the narrow ribbon in $Pb_5Sb_6S_{14}$. The sheets occur in groups of three, two of which grow straight out from parallel narrow ribbons and one of which starts from a truncated wide ribbon after a 120° change in direction. If we label the sheets extended from the narrow ribbons N, and the sheets joining the wide ribbons W, we can describe the structure seen in regions A as . . .N N W N N W. . . . The transformation advances in steps indicated by an arrow in Fig. 4. At the step the sequence of sheets is changed to N N W W N N. There is a noticeable bending of the W-type sheet where it advances deeper into the $Pb_5Sb_6S_{14}$ structure.

In contrast to the pattern in region A, the structures seen in regions B and C, Fig. 5, have grown in the direction of the wide ribbons, but they differ in contrast. In region B, the contrast lines alternate between dark and lighter and they resemble those characteristic of wide ribbons in $Pb_5Sb_6S_{14}$, suggesting that a set of sheets has been formed by extending the wide ribbons. The same type of fringe is seen at the edges of region C, but in the middle of the region all the fringes have the same darkness and approximate spacing, 3 Å, that corresponds to the distance between (002) planes in the stable galena phase of PbS. We infer that near the interface the transformation has started by extending the wide $Pb_5Sb_6S_{14}$ ribbons into sheets but that further away from the inter-

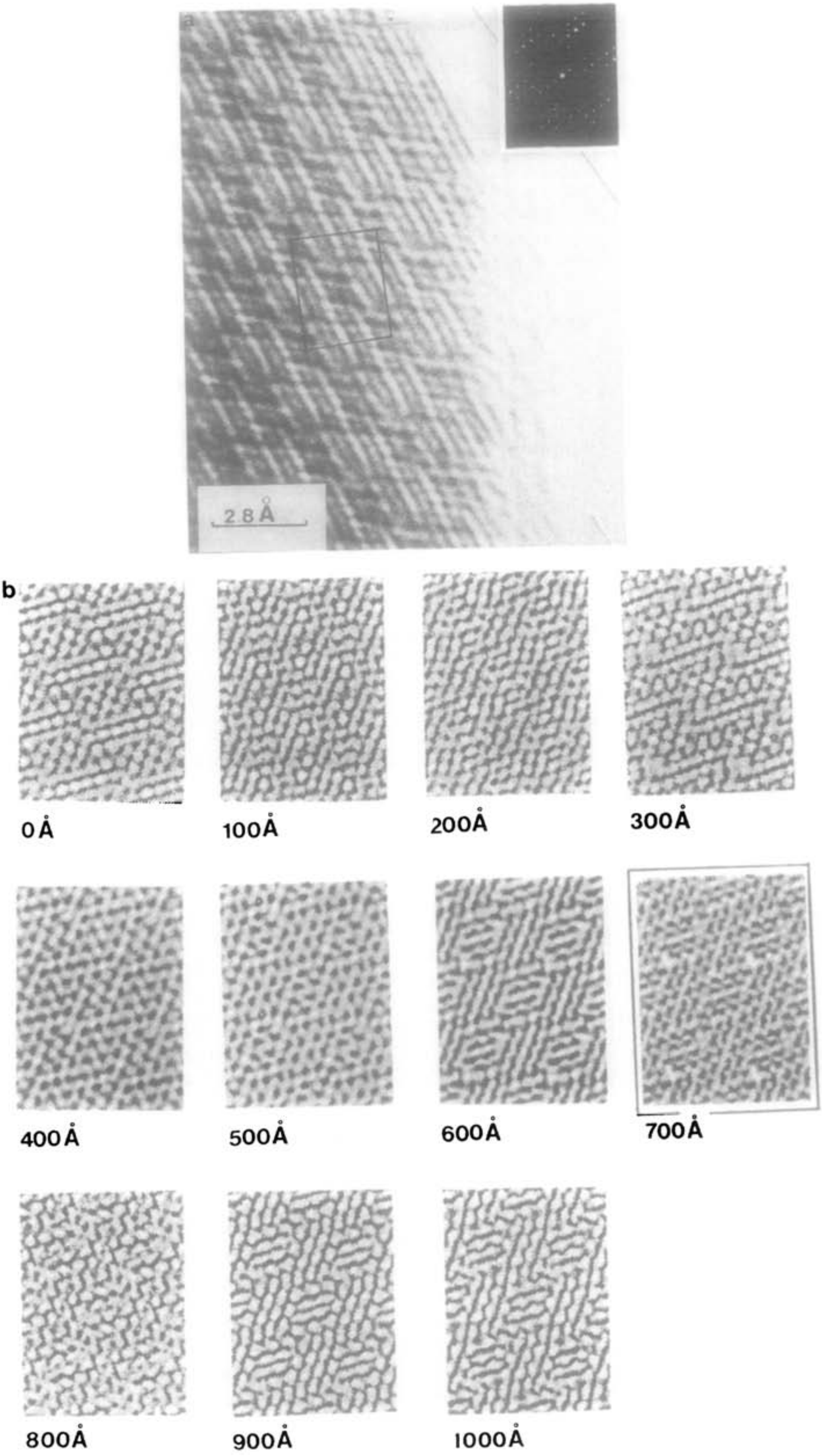
a
28 Å
b
0 Å
100 Å
200 Å
300 Å
400 Å
500 Å
600 Å
700 Å
800 Å
900 Å
1000 Å

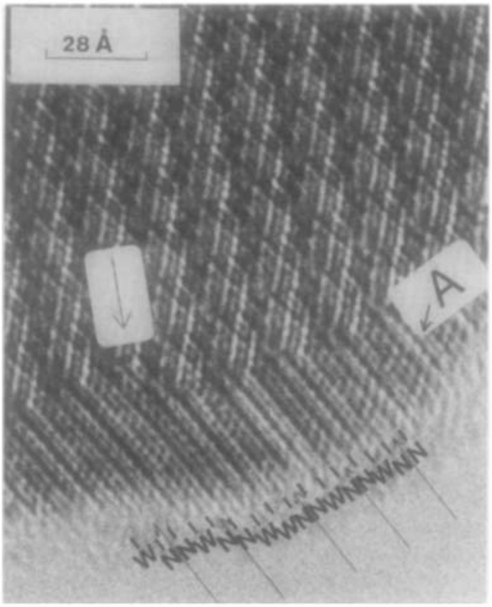

FIG. 4. Electron micrograph of a crystal fragment of $Pb_5Sb_6S_{14}$ which has partly decomposed. The sheets extended from the narrow ribbon are labeled N and the sheets joining the wide ribbon, W. The step in the interface between the transformed and the untransformed part of the crystal is indicated by an arrow.

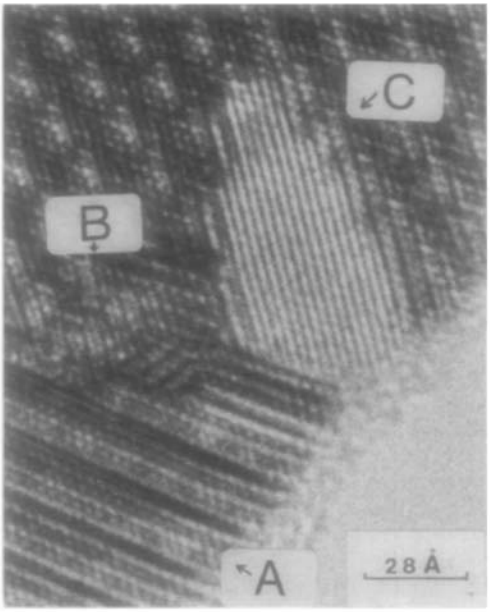

FIG. 5. Electron micrograph of a $Pb_5Sb_6S_{14}$ crystal fragment which has partly decomposed into three structures labeled A, B, and C. Region A is formed by the extension of the narrow ribbons of $Pb_5Sb_6S_{14}$, as in Fig. 4. Regions B and C are formed by extension of the wide ribbons.

face the structure has transformed into galena.

All the observed transformations require severe atomic rearrangements and must occur by recrystallization and growth rather than by small atomic displacements. The transformations result in the formation of wide sheets, which implies either the creation of cation vacancies or a change of stoichiometry to PbS. The latter is more likely, since Sb_2S_3 is more volatile than PbS and the required loss of antimony sulfide can easily occur in the thin parts of the sample exposed to the electron beam. The remaining PbS-rich material recrystallizes using the thicker untransformed parts of the crystal as the seed structure. A number of structures are possible, the stable galena structure, the TlI structure that would be formed by extending the ribbons of $Pb_5Sb_6S_{14}$, or hybrids of these two structures in which only some of the planes are sheared.

The galena and TlI structures have been used to propose models for the decomposition. In region B the wide ribbons of

---

FIG. 3. (a) High resolution electron micrograph of a thin crystal fragment of $Pb_5Sb_6S_{14}$. The structure is projected along [010] and the unit cell is outlined. By comparison with Fig. 2a it can be seen that both wide and narrow ribbons are resolved. (Note that the photograph is inverted.) (b) The calculated images of $Pb_5Sb_6S_{14}$ for the crystal thickness of five unit cells, the objective aperture 100 $Å^{-1}$ and various defocus as indicated. The best fit between the calculated images and those observed at the edges of the crystal is obtained for the defocus of 700 Å.

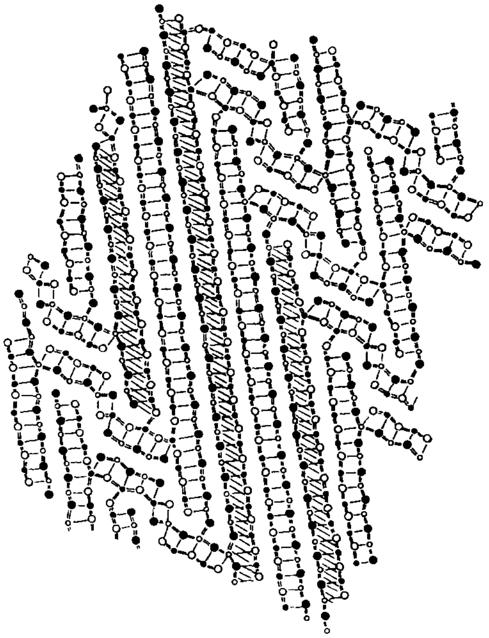

FIG. 6. A model of the structure in region B. The wide $Pb_5Sb_6S_{14}$ ribbons extend coherently into sheets from the crystal. Alternate sheets are shaded.

$Pb_5Sb_6S_{14}$ become extended, and the TlI-type structure proceeds coherently from the crystal to produce a series of widened parallel ribbons as shown in Fig. 6. To model the decomposition in region C we start the transformation by first producing a series of widened TlI type ribbons as in region B. To obtain the galena structure every other sheet is sheared in the *b*-direction by introducing the defects indicated by circles. This is shown in Fig. 7.

Figure 8 shows a model of the decomposition seen in region A. Here, the narrow ribbons extend as pairs of TlI-type sheets. The space between them is filled with a single sheet that connects with the truncated wide ribbon. This gives the sheet sequence . . . N N W N N W. . . . Two models can be proposed for fitting the single, W, sheets between the pairs of N sheets. In the first, the W sheet is fitted without the shear and each Pb has a regular 6 coordination. This gives bands of galena structure separated by a single shear, indicated as ^, e.g., N^NWN^NWN^N. In the second model a pair of shears is introduced into the ^N W N^ bands of galena structure between the N and W sheets, resulting in a uniform region of TlI-type structure, N^N^N^W^N^N^W. The micrographs themselves do not indicate which model is correct, and both models have difficulties. The contrast variation in every third sheet, seen in the region A (particularly in Fig. 5), suggests the first model, with the galena-type stacking of sheets between the shears, but this should result in more uniform contrast within the galena-like bands than is observed in Fig. 4. The second model, with the shears between all the sheets, runs into difficulty at the step in the interface between the crystal and the region

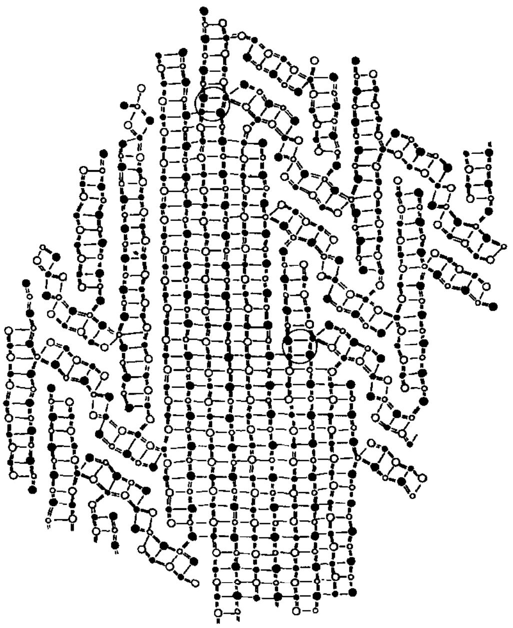

FIG. 7. A model of the structure in region C. Alternate sheets extending from the wide ribbon of $Pb_5Sb_6S_{14}$ (shaded in Fig. 6) are sheared in the *b*-direction to produce the galena structure. The resulting stacking faults are indicated by circles.

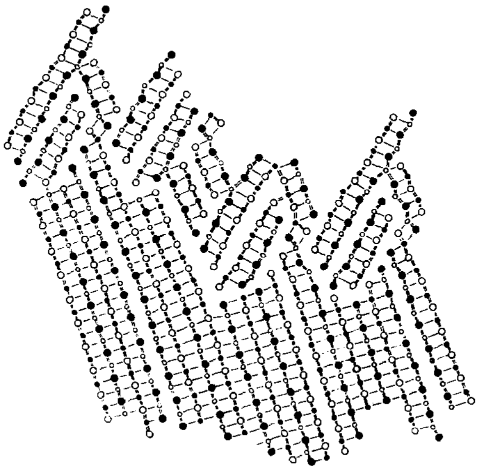

FIG. 8. A model of the structure in region A. The narrow ribbons in $Pb_5Sb_6S_{14}$ are extended into sheets. Only the model in which the bands of galena structure are separated by a single shear, indicated by a long arrow, is drawn. The sheets are bent at the step in the interface between the transformed and the untransformed part of the crystal.

A, since to shear the galena band, ^N W W N^, which occurs there, one has to introduce an odd number of shears, which is impossible. In Fig. 8 we show the arrangement of the ribbons according to the first N^NWN^N model. The bending observed at the step in the interface between the crystal and the region A is reproduced in the drawing.

Acknowledgments

We are indebted to R. Faggiani for help in the single crystal X-ray data collection and to the Natural Science and Engineering Research Council of Canada for an operating grant. A.S. is indebted to I.C.I. and the British Council for financial support in the initial stages of this project. R.J.D.T. is grateful to N. Dodds for assistance in generating the simulated images.

References

1. N. WANG, *Neues Jahrb. Mineral. Abh.* **128,** 167 (1976).
2. "International Tables for X-Ray Crystallography," Vol. 4, Tables 2.2B and 2.3.1, Kynoch Press, Birmingham (1974).
3. A. SKOWRON AND I. D. BROWN, *Acta Crystallogr., Sect. C: Cryst. Struct. Commun.,* **46,** 527 (1990).
4. J. SPENCE, "Experimental High Resolution Electron Microscopy, pp. 102 and 356, Clarendon Press, Oxford (1981).
5. P. BAYLISS AND W. NOWACKI, *Z. Kristallogr.* **135,** 308 (1972).
6. E. MAKOVICKY, *Fortschr. Mineral.* **63,** 45 (1985).
7. P. P. K. SMITH AND B. G. HYDE, *Acta Crystallogr. Sect. C: Cryst. Struct. Commun.* **39,** 1498 (1983).
8. E. MAKOVICKY, *Fortschr. Mineral.* **59,** 137 (1981).
9. L. HELMHOLZ, *Z. Kristallogr.* **95,** 129 (1936).
10. W. HOFMANN, *Z. Kristallogr.* **86,** 225 (1933).
11. H. WIEDEMEIER AND H. G. VON SCHNERING, *Z. Kristallogr.* **156,** 143 (1981).
12. S. DEL BACCHIA, J. C. JUMAS, AND M. MAURIN, *Acta Crystallogr., Sect. B: Struct. Crystallogr. Cryst. Chem.* **37,** 1903 (1980).
13. P. A. STADELMANN, *Ultramicroscopy* **21,** 131 (1987).